JACS
JOURNAL OF THE AMERICAN CHEMICAL SOCIETY
pubs.acs.org/JACS
Article

Kinetics of NH_3 Desorption and Diffusion on Pt: Implications for the Ostwald Process

Dmitriy Borodin, Igor Rahinov, Oihana Galparsoro, Jan Fingerhut, Michael Schwarzer, Kai Golibrzuch, Georgios Skoulatakis, Daniel J. Auerbach, Alexander Kandratsenka, Dirk Schwarzer, Theofanis N. Kitsopoulos,* and Alec M. Wodtke*

Cite This: J. Am. Chem. Soc. 2021, 143, 18305−18316

Read Online

ACCESS | Metrics & More | Article Recommendations | Supporting Information

ABSTRACT: We report accurate time-resolved measurements of NH_3 desorption from Pt(111) and Pt(332) and use these results to determine elementary rate constants for desorption from steps, from (111) terrace sites and for diffusion on (111) terraces. Modeling the extracted rate constants with transition state theory, we find that conventional models for partition functions, which rely on uncoupled degrees of freedom (DOFs), are not able to reproduce the experimental observations. The results can be reproduced using a more sophisticated partition function, which couples DOFs that are most sensitive to NH_3 translation parallel to the surface; this approach yields accurate values for the NH_3 binding energy to Pt(111) (1.13 ± 0.02 eV) and the diffusion barrier (0.71 ± 0.04 eV). In addition, we determine NH_3's binding energy preference for steps over terraces on Pt (0.23 ± 0.03 eV). The ratio of the diffusion barrier to desorption energy is ∼0.65, in violation of the so-called 12% rule. Using our derived diffusion/desorption rates, we explain why established rate models of the Ostwald process incorrectly predict low selectivity and yields of NO under typical reactor operating conditions. Our results suggest that mean-field kinetics models have limited applicability for modeling the Ostwald process.

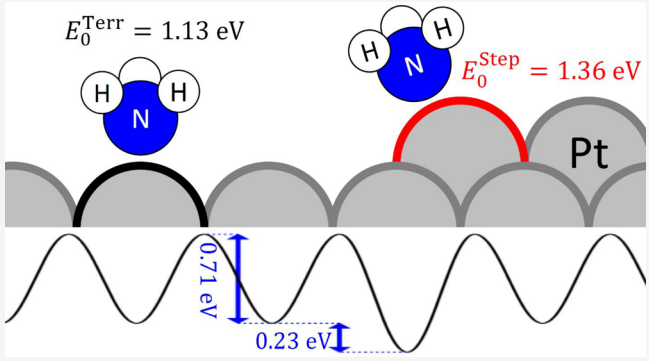

1. INTRODUCTION

The Ostwald process is a critically important stepping stone for industrial production of artificial fertilizers, converting ammonia (NH_3) to nitric acid (HNO_3) in the presence of oxygen and water. The key to its success is the efficient oxidation of NH_3 to nitric oxide (NO) on a Pt catalyst. In industry, the Ostwald process is conducted at temperatures of 1050−1250 K and total pressures between 1 and 12 bar with an ammonia to air ratio of 1:10.[1] To initiate the oxidation, NH_3 adsorbs with high probability to the majority terrace site and must then diffuse to low-coordination step sites, where it is able to react with oxygen.[2−8] Thus, the competition between desorption and diffusion and the equilibrium between adsorption at step and terrace sites are critical factors in determining reaction probability; yet the competition between NH_3 desorption and diffusion on Pt has never been investigated. There is not even an experimental consensus concerning such a basic parameter as the binding energy of NH_3 at Pt(111). Molecular beam relaxation spectrometry (MBRS)[9] yielded a binding energy of 0.68 eV, whereas analysis of collision-induced desorption (CID) experiments[10] led to a value of 1.1 eV. Laser-induced desorption (LID)[11] studies suggest a binding energy of ∼0.8 eV, consistent with results obtained with temperature-programmed desorption (TPD).[12,13] Analysis of TPD data also reveals a weakening NH_3−Pt bond with increasing NH_3 coverage and contradicts the expectation one might infer from MBRS, conducted at low coverages, and CID, conducted at high coverages. Obviously, the uncertainty among the experimental determinations of the binding energy precludes any serious comparison with theory. This is presumably the reason why the NH_3 binding energy at Pt(111), despite its importance, is still missing from experimental benchmark tables.[14] Furthermore, real catalysts exhibit a diversity of active sites, including steps and kinks, and the relative binding strengths of molecules to different sites can determine the reactant's ability to compete with other molecules to occupy the active site(s). Sadly, no reliable site-specific binding energies of NH_3 on Pt have yet been reported.

The lack of reliable quantitative information concerning NH_3/Pt interactions led to surrogate empirically optimized models, which unfortunately lack universality and trans-

Received: September 1, 2021
Published: October 21, 2021

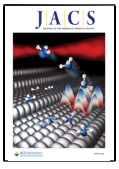

ACS Publications
© 2021 The Authors. Published by American Chemical Society

https://doi.org/10.1021/jacs.1c09269
J. Am. Chem. Soc. 2021, 143, 18305−18316

ferability. Nevertheless, the Ostwald process has been modeled using transition state theory (TST) and density functional theory (DFT) to calculate the relevant rate parameters on single crystal model catalysts like Pt(111),[2,15] Pt(100),[16] and Pt(211)[2,4,17] that are then used to elucidate the optimum process conditions. Such models have rarely been validated by comparison to experiment, of which there are few. One of the best known models, frequently used in reactor simulations of the Ostwald process, was developed by Kraehnert and Baerns[18] (KB). The KB kinetics model relies on a mechanism derived from DFT calculations on Pt(111) by Offermans et al.[15] and optimizing the rate parameters to achieve agreement with the experimental rates of NH_3 oxidation on polycrystalline Pt at 1 mbar and 600 K. Experimental observations could only be explained assuming that adsorbed NH_3 (NH_3*) and O* occupy different binding sites. These sites were assigned to those found on Pt(111) single crystals—on top for NH_3* and fcc hollow for O* and NO*.[18] Other structural features like steps, which are known to be more reactive than terraces,[2,6,7] were not considered. Scheuer et al. pointed out that the KB mechanism lacks quantitative transferability to the ammonia slip[19] regime, where NH_3 reacts with O_2, forming predominantly N_2 and H_2O. The lack of transferability is likely due to the use of rate constants, which do not reflect the correct elementary processes. For example, the KB mechanism includes a 0.65 eV adsorption barrier for NO on Pt, in contradiction to our current understanding that NO−Pt adsorption is barrierless.[20,21] Beyond this, the rate parameters used to describe NH_3 desorption in the KB model include an unphysically low prefactor in the Arrhenius expression, suggesting the entropy of Pt-adsorbed NH_3 is higher than that of the gas-phase molecule. Clearly, there is a pressing need for reliable information on site-specific binding energies and entropies of NH_3 and other molecules on Pt surfaces.

In this work, we report elementary thermal rate constants for NH_3 desorption from and diffusion on Pt(111) and Pt(332) at surface temperatures $430 \leq T \leq 620$ K, derived from kinetic data obtained with the velocity-resolved kinetics method.[22] We find that the kinetic traces for the desorption rate of NH_3 from a Pt(111) surface do not follow first-order kinetics but are instead biexponential. This is attributed to the exceptionally high diffusion barrier of NH_3 on the (111) terrace that slows down the diffusion across the terraces toward the steps: molecules that desorb from the terrace prior to reaching the steps comprise the fast component of the biexponential, whereas molecules that make contact with the steps comprise the slow component. We globally fit desorption data from Pt(111)—step density 0.4 ± 0.2% monolayer (ML)—and Pt(332)—step density 16.7%ML—using a kinetics model that includes NH_3* desorption from terraces and steps, hopping across terraces and hopping from steps to terraces. From the derived rate constants, we can accurately compute the desorption rate of NH_3 from Pt surfaces as well as the population of step and terrace sites as a function of step density, pressure, and temperature.

The high quality of the kinetic data over a wide range of temperatures provides a great deal of information through application of TST, but the most common implementations of TST reported so far cannot reproduce our results. This problem is solved by developing a semiempirical partition function of adsorbed ammonia that includes the coupling between several modes that actively participate in diffusion. Using this form of TST, we obtain an excellent fit to the measured rate constants as well as NH_3's binding energy on terraces of Pt(111) (1.13 ± 0.02 eV), the diffusion barrier between binding sites of Pt(111) (0.71 ± 0.04 eV), and the degree of energetic stabilization of NH_3 at steps compared to terraces (0.23 ± 0.03 eV). These results are in good agreement with DFT calculations that we also report here. Note the diffusion barrier for this system is ∼65% of the binding energy, a strong violation of the so-called 12% rule,[23,24] postulating that diffusion barrier constitutes a rather small fraction of a binding energy. Clearly, the 12% rule should be used with caution.

We also used DFT calculations to investigate the coverage dependence of the NH_3 desorption rate; our results are able to reproduce previously reported TPD experiments carried out for NH_3/Pt(111),[12] conducted at much lower surface temperatures. This success of our approach over such a wide temperature range justifies modeling catalyst NH_3 coverages at high temperatures and pressures typical for Ostwald catalysis reactors. Our model predicts NH_3 coverages below ∼10%, whereas established reactor models predict fully covered catalysts at all conditions relevant to the Ostwald process. We believe this explains why some of the established reactor models tend to overestimate the degree of NH_3 slippage at process-relevant conditions.[18] Finally, we find that the derived desorption and diffusion rates from this work suggest that the mean-field approximation, frequently employed to model reaction rates, is not appropriate for description of NH_3 reactivity on Pt under industrially relevant conditions.

2. RESULTS

The velocity-resolved kinetics technique has been described in detail elsewhere.[22,25,26] Compared to other kinetics methods applied to surface processes, it has the advantage of providing time-resolved desorption flux directly, as NH_3's velocity- and angle-resolved density is obtained as a function of its surface residence time using ion imaging. Briefly, NH_3 is deposited at a Pt surface of known temperature using a short (∼35 μs) molecular beam pulse to initiate the thermal desorption process. The flux of desorbing ammonia ($\propto d[NH_3^*]/dt$) is obtained as a function of residence time by scanning the delay between the molecular beam pulse and an ionization laser pulse. The beam-laser delay is easily converted to surface residence time through knowledge of the molecule's speed. Together this yields the kinetic trace, defined as the flux of ammonia leaving the surface versus residence time. At each value of time, velocity-resolved kinetics provides not only the kinetic trace but also, in addition, the speed and angular distributions of the desorbing ammonia molecules. See section 5.1 for further details of the methods used for these measurements.

We obtained the speed distributions for NH_3 desorption from both Pt(111) and (332) at several surface temperatures, T_S (Supporting Information (SI), section S1). We fit these to Maxwell−Boltzmann distributions, extracting an effective translational temperature for the desorbing molecules, T_{tr}. For experiments with Pt(332), T_{tr} was found to be equal to T_S; whereas, for Pt(111) T_{tr} was less than T_S. Based on detailed balance,[27] these results immediately indicate that NH_3 adsorption to Pt has no activation barrier and, therefore, that the binding energy is equal to the desorption energy. Furthermore, we also obtain the shape of the sticking probability curve as a function of kinetic energy $S(E_{tr})$, and by assuming $S(E_{tr} = 0)$ to be 1,[28] we obtain the absolute

https://doi.org/10.1021/jacs.1c09269
J. Am. Chem. Soc. 2021, 143, 18305−18316

quantity $S(E_{tr})$. This is used to obtain the thermal sticking probability $\langle S_0 \rangle(T)$ between 0 and 2000 K, which is shown in section S2 in the SI. A previous report at a single temperature[9] agrees well with our results.

We also obtained kinetic traces for NH_3 desorption from Pt(111) and Pt(332), which are shown on a logarithmic scale at nine surface temperatures in Figure 1. The sharp, early time

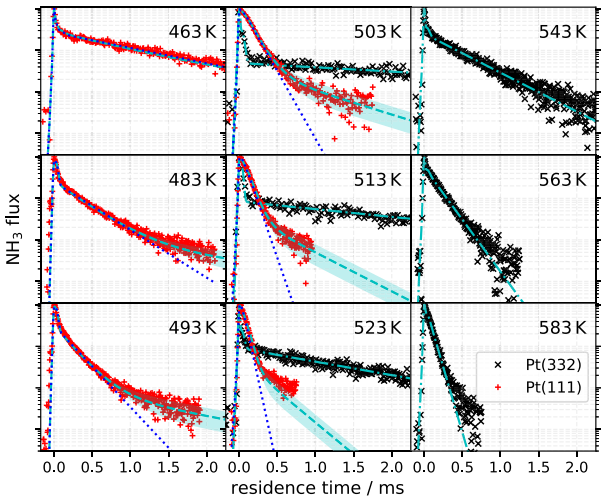

Figure 1. Kinetic traces of NH_3 desorbing from Pt(111) (+) and Pt(332) (×) for surface temperatures between 463 and 583 K. The step density of the Pt(111) is 0.4 ± 0.2%ML and of Pt(332) is 16.7% ML. The light blue dashed (− −) and dash-dotted (− · −) lines show the global fit to the experimental kinetic data for Pt(111) and Pt(332), respectively. The shaded regions indicate the model uncertainty associated with the step density of the Pt(111) surface. The blue dotted line (···) indicates the model's prediction for NH_3 desorption rate from a step-free (ideal) Pt(111) surface.

(first 0.1 ms) feature is a residual NH_3 background from the directly scattered beam. It is independent of surface temperature and exhibits a narrow angular distribution peaking close to the specular angle. The dominant contribution to the observed signal is temperature-dependent and arises from thermally desorbing NH_3. It has a broad angular distribution ($\sim\cos(\theta)$), where θ is the angle with respect to the surface normal. The NH_3 desorption rate from Pt(332) follows first-order kinetics as expected for a simple desorption process; however, NH_3 desorbing from Pt(111) with 0.4 ± 0.2% steps is biexponential, with a fast (major) and a slow (minor) component. We repeated the desorption experiments at a Pt(111) surface with fewer steps and found that the slow component could be even further reduced (see section S3 in the SI). Notice that, when compared at the same temperature, the major component of Pt(111) data is faster than desorption from Pt(332). This indicates that NH_3 has an increased residence time on highly stepped surfaces.

Figure 2 shows schematically the energy landscape and key elementary processes, with their rate constants, of a kinetics model capable of describing NH_3 diffusion and desorption at Pt surfaces as a function of step density. The model is one-dimensional describing diffusion perpendicular to steps only. Each rate constant is parametrized in an Arrhenius form. The short time behavior of the kinetic trace, representing the direct scattering, is modeled with a temperature-independent model based on the arrival time distribution of the NH_3 at the surface. We use periodic boundary conditions and make the model

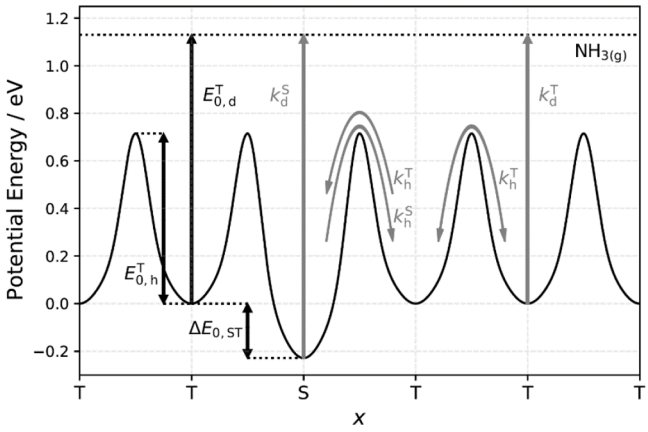

Figure 2. Schematic overview of the elementary processes (gray) included and energy parameters (black) extracted from the desorption−diffusion kinetics model. Steps and terraces are indicated by the letter S and T, respectively. The NH_3 binding energy at (111) terraces of Pt is $E^T_{0,d}$ = 1.13 ± 0.02 eV, the site-to-site hopping barrier is $E^T_{0,h}$ = 0.71 ± 0.04 eV, and the energy preference for steps is ΔE_{ST} = 0.23 ± 0.03 eV. Following a similar strategy as described in ref 20, we include five elementary processes with first-order rate constants: (1) hopping between adjacent terrace sites, k^T_h; (2) hopping from terrace to step sites, which is assumed to be the same as k^T_h; (3) hopping from step to terrace sites, k^S_h; (4) desorption from terrace sites k^T_d; and (5) desorption from step sites, k^S_d. We note that k^S_d describing process (5) is not an independent rate constant, $k^S_d = k^T_d k^S_h / k^T_h$; see section S4.1 of the SI.

applicable to different step densities by varying the number of terrace sites separating the steps. Using this diffusion−desorption kinetics model (see section S4.2 of the SI for details), we fit the measured desorption rates from Pt(111) and Pt(332) simultaneously at all temperatures (see section S4.3 of the SI for details). The fit, shown as dashed (− −) and dash-dotted (− · −) lines in Figure 1, is excellent. The six independently derived Arrhenius rate parameters and their uncertainties are presented in Table 1.

Using the values of Table 1, we simulated how NH_3 desorption would look in the absence of steps (blue dotted

Table 1. Rate Constants for Desorption and Diffusion of Ammonia on Platinum[a,b]

elementary rate constants	fitted parameters	fit results
$k^T_d(T)$	$E^T_{a,d}$/eV	1.09 ± 0.02
	$\log_{10}(A^T_d/s^{-1})$	14.8 ± 0.2
$k^S_h(T)$	ΔE_{ST}/eV[c]	0.23 ± 0.03
	$\log_{10}(A^S_h/s^{-1})$	13.7 ± 0.6
$k^T_h(T)$	$E^T_{a,h}$/eV	0.73 ± 0.04
	$\log_{10}(A^T_h/s^{-1})$	13.6 ± 0.4
	derived quantities	
$k^S_d(T) = k^T_d k^S_h / k^T_h$	$E^S_{a,d}$/eV	1.32 ± 0.04
	$\log_{10}(A^S_d/s^{-1})$	14.9 ± 0.6
$D^T(T)$[d]	$\log_{10}(D^T_0/cm^2\ s^{-1})$	−1.9 ± 0.4

[a]Results were obtained from the global fit of the kinetics model to experimental desorption rates from Pt(111) and Pt(332). [b]The elementary rate constants are parametrized according to the Arrhenius equation: $k(T) = A \exp(-E_a/k_B T)$. [c]$E^S_{a,h} = E^T_{a,h} + \Delta E_{ST}$. Since $A^S_h \approx A^T_h$, the difference of activation energies ΔE_{ST} is nearly equal to the difference of binding energies $\Delta E_{0,ST}$. [d]$D^T(T) = D^T_0 \exp\left(-\frac{E^T_{a,h}}{k_B T}\right)$, where D^T_0 is derived from A^T_h following ref 29.

https://doi.org/10.1021/jacs.1c09269
J. Am. Chem. Soc. 2021, 143, 18305−18316

lines (···) in Figure 1). This shows that the fast component of the biexponential decay reflects direct desorption from terrace sites. In light of the relatively large step stabilization energy ΔE_{ST} also shown in Table 1, it becomes clear why desorption from Pt(332) is slower than the fast component of desorption from Pt(111). Table 1 also shows the computed prefactor for the terrace diffusion constant $D^{T}(T)$ derived from the hopping rate constant $k_h^T(T)$ following ref 29 as well as the rate constant for direct desorption from steps $k_d^S(T)$, which is derived from the other rate constants. Notice that the Arrhenius prefactor for terrace desorption and direct step desorption are nearly equal; that is, the entropy of the NH_3 is nearly the same for these two binding sites. This is a striking result and means that the ammonia molecule is highly localized at terrace sites, a conclusion that is consistent with the large activation energy found for terrace hopping $E_{a,h}^T = 0.73 \pm 0.04$ eV.

Combining kinetic data with DFT parametrized TST can be highly useful. Thus, we performed a variety of DFT calculations using the Perdew−Burke−Ernzerhof (PBE) exchange-correlation functional.[30] Our experiments are relevant to the zero-coverage limit; hence, we relied most heavily on DFT calculations carried out using a periodic 4 × 4 unit cell. We find that the on-top site is the most stable binding site for NH_3* at Pt(111) with a (zero-point energy corrected) binding energy of 0.86 eV at 0.06 ML. In addition, we performed calculations with 2−4 NH_3* molecules placed in the cell to produce coverages from 0.12 to 0.25 ML. We calculated the NH_3* binding energy at Pt(111) in each case and find it to decreases linearly with increasing coverage with a slope of $\alpha = -1.61$ eV/ML. Based on this finding, we determine a zero-coverage binding energy of 0.95 eV (see section S5 of the SI). Similarly, we calculate the binding energy at Pt(332) and, by comparison to Pt(111), find that the step stabilization is 0.30 eV.

In addition to the binding energy calculations, we performed analysis of the minimum energy pathway for hopping between on-top binding sites of Pt(111). We use the climbing image nudged elastic band (CI-NEB) method[31] to locate the TS that we found at the bridge site. We obtain a zero-point energy corrected hopping barrier of 0.70 eV (0.52 eV) for the 4 × 4 (2 × 2) supercell. We also performed calculations of the harmonic frequencies at the on-top most stable binding site and for the transition states found at the bridge site (see Table 2).

3. FURTHER ANALYSIS AND DISCUSSION

3.1. Two Approaches to the Adsorbate Partition Function. In this section, we analyze the derived thermal rate constants in terms of transition state theory. This allows us to derive fundamental quantities such as the desorption energy and the diffusion barrier height. We elaborate detailed expressions for the adsorbate partition function in two ways. The partition function is normally considered a product of partition functions for the individual degrees of freedom (DOFs). We show here that this uncoupled TST approach fails to reproduce our experimental results. We then introduce a partition function which makes a better accounting of the state count when some of the DOFs are coupled (coupled TST). Coupled modes are identified through DFT calculations of NH_3's minimum energy pathway for hopping where we find that hindered translation and frustrated rotational modes are actively participating in the site-to-site exchange. This is reflected by an increase of surface−molecule distance and tilting of NH_3's symmetry axis along the minimum energy pathway. Also the associated vibrational frequencies decrease at the transition state for hopping by a factor of 2 to 3 (see Table 2), reflecting their importance for accurate description of the adsorbate entropy. This approach allows us to explain the temperature dependence of the rate constants precisely over the entire temperature range. This then provides the most accurate energy barriers for NH_3 site-to-site hopping and desorption from Pt(111) presently available.

Table 2. Results of DFT Calculations Performed for This Work: Harmonic Frequencies for NH_3* at the Most Stable Binding Site (On-Top) and on the Transition State (TS) for Hopping (Bridge) Obtained from a 4 × 4 [2 × 2] Supercell Using the PBE Exchange-Correlation Functional[a]

mode		calculated harmonic frequencies/cm^{-1}	
ν_i (ν_{gas})	description	on-top	TS for hopping (bridge)
ν_1 (3a)	asym. stretch	3483.1 [3484.4]	3546.7 [3550.5]
ν_2 (3b)	asym. stretch	3481.5 [3482.8]	3540.1 [3545.6]
ν_3 (1)	sym. stretch	3356.8 [3342.7]	3400.6 [3397.4]
ν_4 (4a)	asym. bending	1572.5 [1551.3]	1583.3 [1586.8]
ν_5 (4b)	asym. bending	1571.5 [1549.7]	1581.3 [1577.9]
ν_{umb} (2)	umbrella mode	1142.0 [1055.2]	930.0 [856.2]
	free C_3-axis rotation	- [-]	- [-]
R_x	frustrated rotation	672.7 [636.3]	325.8 [131.3]
R_y	frustrated rotation	672.4 [636.3]	269.9 [109.5]
T_z	hindered translation	357.8 [338.3]	127.5 [45.9]
T_x	hindered translation	122.8 [109.5]	190.9i [176.4i]
T_y	hindered translation	119.9 [109.5]	68.2 [-]

[a]The imaginary frequency in T_x at the TS emerges from the degeneracy with the hopping coordinate. In this work we numbered the internal modes of adsorbed NH_3 from high to low frequency. The conventional nomenclature from gas-phase vibrational spectroscopy is provided in parentheses for convenience.

The general expression for the TST rate constant for desorption or diffusion is

$$k_{TST}(T) = \frac{k_B T}{h}\frac{Q^{\ddagger}}{Q_{ad}}\exp\left(-\frac{E_0}{k_B T}\right) \quad (1)$$

where Q_{ad} is the partition functions of the ammonia adsorbate, $Q^{\ddagger}$ is the partition function for the transition state, and E_0 is the zero-point energy corrected barrier height. Highly accurate evaluation of Q_{ad} is often unnecessary in analyzing surface desorption rate data as the uncertainty in the experimental prefactor often exceeds an order of magnitude[32] or in many cases is not measured at all.[8] When analyzing high-quality kinetic data as obtained with velocity-resolved kinetics, Q_{ad} becomes a sensitive probe of the NH_3/Pt interactions. Inappropriate approximations lead to detectable deviations from the measured desorption rates. In the following, we demonstrate the deficiencies of uncoupled TST and the advantages of coupled TST for the computation of Q_{ad}.

The first approach, uncoupled TST (uTST), uses a sophisticated and established approach. Here, we base it on the approximation of a hindered translator,[33] which is considered as one of the more accurate ways to compute Q_{ad}.[34] Here, the partition functions for $T_{x,y}$ are described using a model potential, parametrized using DFT-calculated hindered translational frequencies (see Table 2) and the

https://doi.org/10.1021/jacs.1c09269
J. Am. Chem. Soc. 2021, 143, 18305−18316

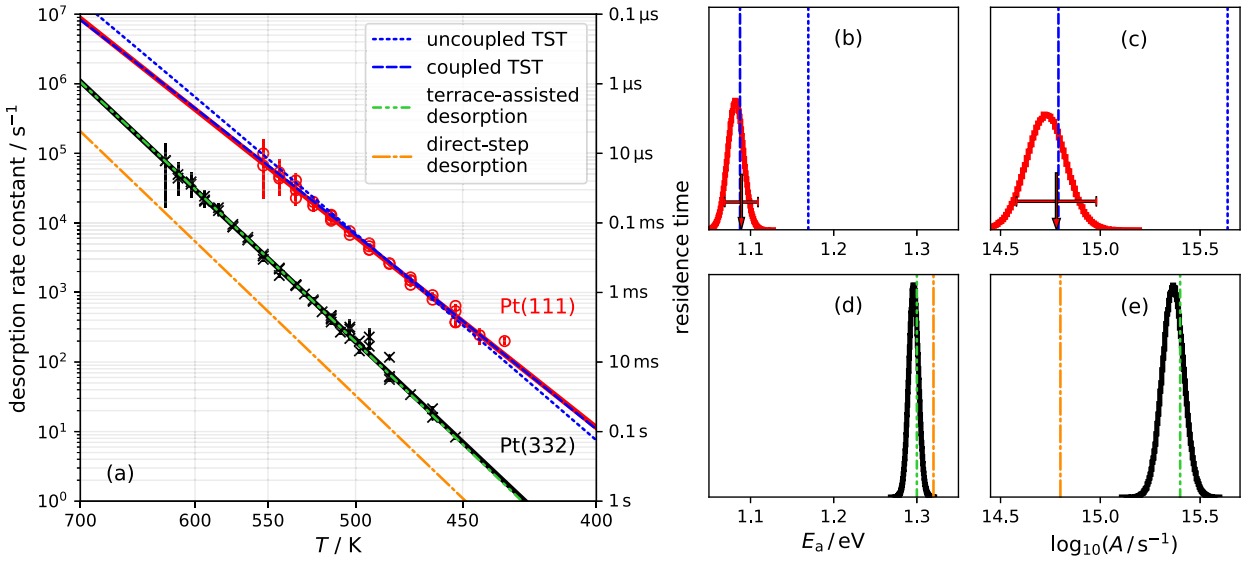

Figure 3. (a) NH_3 desorption rate constants from Pt(111) terrace obtained from global kinetics model fit (red line) and from individual fits of the kinetic traces (red circles with error bars; see section S7 of the SI). The red line is *not* the Arrhenius fit to the circles. Terrace desorption rate constants are compared to the uTST (blue dotted) and cTST (blue dashed) models. The first-order desorption rate constants from Pt(332) (black crosses with error bars) and the corresponding Arrhenius fit (solid black line) are compared with a model assuming that desorption happens directly from steps (k_d^S from Table 1, orange dash-dotted line) and a model that describes desorption as a "terrace-assisted" process including desorption from terraces and steps (eq 4, green dash-dot-dotted line). (b,c) Comparison of experimentally derived Arrhenius activation energy and prefactor for terrace desorption from Pt(111) and Arrhenius parameters predicted based on uTST (dotted blue line) and cTST (blue dashed line) models at 530 K (average temperature of present experiments). The red arrows with error bars result from global fit of diffusion−desorption kinetics model to experimental data (see SI section S4.3) and are represented by the red line in panel (a). The red histograms are parameter distributions emerging from Arrhenius fit (not shown for clarity) to red circles of panel (a). (d,e) Comparison of the Arrhenius parameter obtained from first-order desorption rate constants from Pt(332) to rate parameters based on direct-step and "terrace-assisted" desorption model at 530 K.

experimentally derived terrace hopping barriers (see section 3.3). The hindered translational partition function exploits an established interpolation scheme, ensuring its proper behavior at low and high temperatures.[21,33,35] We treat NH_3 rotation around its symmetry axis as a free rotation, justified by our DFT results and in agreement with previous theoretical work.[36] The remaining DOFs are described by harmonic oscillators. For uTST, we use DFT-calculated frequencies for NH_3 bound at its most stable binding site (see Table 2), consistent with how this approach is conventionally applied (for further details, see section S6.1 of the SI).

The uTST assumes that all DOFs are decoupled, making Q_{ad} a product of the partition functions of each DOF sensitive only to the structure of the molecule at the on-top binding site. However, when NH_3* migrates over a diffusion barrier, its binding strength at the surface weakens, and consequently, the vibrational modes, especially those that strongly influence the oriented molecule−surface binding ($R_{x,y}$, T_z, and ν_{umb}), soften substantially (see Table 2). Since these modes have low frequencies, further frequency reduction has a large impact on the thermally accessible density of states.

To account for this effect, we developed a second approach, dubbed hereafter as the coupled TST (cTST) model. Briefly, cTST allows translation parallel to the surface to explicitly soften several of ammonia's vibrational frequencies. This precludes a product form for Q_{ad}. Instead, we construct a partition function where the vibrational frequencies of several modes (ν_{umb}, R_x, R_y, and, T_z) vary along the minimum energy pathway for site-to-site hopping. This approach describes more faithfully the bond softening induced by the motion toward the diffusion barrier. Other DOFs are described as in uTST model. The construction of Q_{ad} for the cTST is described in detail in the SI section S6.2. In the next section, we apply uTST and cTST for the description of desorption and hopping rates of NH_3 at Pt(111).

3.2. Analysis of the Desorption Rate Constants Using TST. To obtain desorption rate constants from TST, we must compute $Q^{\ddagger}$. The modern formulation of TST prescribes a dividing plane that separates reactants from products such that every trajectory that originates in the reactant region of configuration space and evolves to the product region must pass through the dividing plane at least once. The choice of the position of the dividing plane can influence the probability for recrossing, which introduces a recrossing error to the TST rate. For NH_3 desorption from Pt, it is convenient to place the dividing plane far from the surface, where the gas-phase NH_3 molecule becomes the transition state. This choice of the transition state is convenient, as the thermal sticking coefficient $\langle S_0 \rangle(T_S)$ obtained above serves as the exact recrossing correction.[37] Furthermore, $Q^{\ddagger}$ is easily computed using tabulated gas-phase vibrational frequencies and rotational constants. We carried out this procedure in a similar way to a recent report for NO desorption from Pd;[21] also, see section S6.3 of the SI.

We may then write down a highly accurate formula for the experimentally derived desorption rate constants:

$$k_d(T) = \langle S_0 \rangle(T) k_{TST}(T) \quad (2)$$

Using eq 2, we optimized E_0 to fit the cTST and uTST model to the experimentally derived terrace desorption rate constants—red circles with error bars and solid red line in Figure 3a. The red line is the terrace desorption rate constant that we extract from the global kinetics model fit (see also Table 1). Complementary to the global fit results, we analyze

https://doi.org/10.1021/jacs.1c09269
J. Am. Chem. Soc. 2021, 143, 18305−18316

the fast decay of each NH_3 kinetic trace from Pt(111) that we assigned to reflect the terraces' desorption (see Figure 1) and derive the red circles from Figure 3a; see section S7 of the SI for details. The cTST (uTST) yields the blue dashed (dotted) line in Figure 3a with $E^{T}_{0,d}$ = 1.13 ± 0.02 (1.17) eV. Figure 3b,c offers a clear comparison of the cTST and uTST models to the derived Arrhenius rate parameters, which accurately represent the experimental rate constants. Here, the red arrow with the error bar represents the experimental uncertainty of the Arrhenius activation energy (Figure 3b) and Arrhenius prefactor (Figure 3c) for terrace desorption obtained from the global kinetics model fit to the experimental data, see section S4.3 of the SI for details. Complementing this, the red histograms display the uncertainty of the terrace desorption Arrhenius rate parameters that we derive from an Arrhenius fit (omitted in Figure 3a for clarity) to the red circles from Figure 3a. Both rate parameters are accurately reproduced by the cTST model (blue dashed vertical line), while the uTST model (blue dotted vertical line) clearly fails. Specifically, the uTST predicts an adsorbate entropy that is too low, and thus the resulting prefactor is too high (Figure 3c). The activation energy is then forced to be artificially high to compensate for this error in the prefactor (Figure 3b).

Based on this analysis, we recommend the results of the cTST model ($E^{T}_{0,d}$ = 1.13 ± 0.02 eV) for future use as the ammonia desorption energy on Pt(111). This value agrees with results from CID[10] (1.1 ± 0.1 eV), although the error bar of that work was far outside chemical accuracy. Results from LID (0.8 eV) are clearly incompatible with the present work.[11] This is likely due to the fact that those experiments were done at relatively high coverages. Despite working at low coverages, previous MBRS results (0.68 eV) are also incompatible with our results. The value of $E^{T}_{0,d}$ found with velocity-resolved kinetics is in poor agreement with DFT calculations when a PBE exchange-correlation functional is used—0.95 eV—see section S5 of the SI. Previous work with the PW91 functional[38] yielded a value of ∼1.0 eV, which agrees only slightly better with the present results, confirming similarities between the PBE and the PW91 functionals.[14]

In the global fit of the kinetics model, we have also derived ΔE_{ST}, the activation energy difference between desorption of NH_3 at steps and terraces of Pt. As these two processes exhibit nearly the same prefactor, the difference of activation energies can be set equal to the difference in binding energies, $\Delta E_{0,ST}$ = 0.23 ± 0.03 eV. This compares well to previous TPD work (∼0.2 eV)[8] and our DFT calculations, which predict an energy preference at steps of 0.3 eV. These results also have implications for the mechanism of desorption from steps. In Figure 3a, we compare a model that naively assumes desorption from a stepped surface, like Pt(332), that occurs directly—that is, diffusion from steps to terraces is unimportant. This clearly fails to capture the experimental observations (orange lines in Figure 3a,d,e). This suggests a more intricate step desorption mechanism, where both steps and terraces play a role. This is discussed further in section 3.5.1.

3.3. Analysis of the Hopping Rate Constants Using TST. We also used the cTST and uTST models to describe NH_3 site-to-site hopping on Pt(111). Here, we require the partition function of the hopping TS. To compute that, we approximate all but two DOFs as simple harmonic oscillators (with frequencies from Table 2). The exceptions are the NH_3* rotation around its symmetry axis, which is again assumed to be a free rotation, and T_y, which is treated as described in section S6.4 of the SI. Note that translation along x drops out, as this is the hopping coordinate. We first carry out this calculation using the DFT-derived and zero-point energy corrected hopping barrier of 0.70 eV presented above. The modeled cTST and uTST hopping rate constants at Pt(111) are shown as blue dashed and blue dotted lines of Figure 4, respectively, and are compared to the experimentally derived hopping rate constant (black solid line).

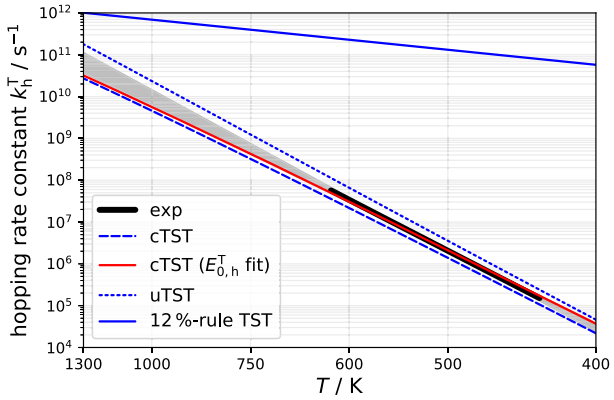

Figure 4. Broad black line shows the derived hopping rate constants in the temperature range of our experiments. The extrapolation of the derived hopping rate constant based on its Arrhenius parameters is shown as the gray shaded region that indicates the uncertainty of extrapolation. The blue solid line is the result of the hopping rate constant that is estimated based on the 12% rule (eq 3) suggested by Mavrikakis and co-workers.[23,24] The blue dashed (dotted) line is the result of cTST (uTST) modeling of hopping rate constant using DFT-calculated hopping barriers. The red solid line is the cTST model using the hopping barrier fitted to the experimental rate constant. The residual mismatch between experiment and the cTST model can be explained with uncertainties in the assumptions of the TS partition functions (see text).

Again, cTST results are within ∼30% of the experimental values. The uTST model predicts rate constants that are systematically ∼2× too large. We note that the residual error in the cTST rate constant is not necessarily due to an error in the DFT barrier height. Instead, it could be an indication that a coupled partition function for the transition state is also required, something that is beyond the scope of this work. Coupling DOFs in the TS would increase TS state densities and increase the hopping rate constant, possibly leading to better agreement with the experiment. The use of an uncoupled partition function for the TS is also likely to be the reason why the deviation of uTST from experiment is only a factor of ∼2—due to a compensation of errors taking place in Q_{ad} and $Q^{‡}$.

We used two approaches to attempt an experimental determination of the hopping barrier. In the first, we optimized $E^{T}_{0,h}$ in the cTST model to fit our experimental hopping rate constant (black solid line of Figure 4). This led to 0.68 eV, which represents a lower limit. See also the red solid line in Figure 4. In the second approach, we used the DFT hopping barrier and determined the difference between activation energy and barrier height for hopping, based on the cTST model; $E^{T}_{a,h}$(500 K) − $E^{T}_{0,h}$ = 0.017 eV, which we subtracted from the experimentally obtained activation energy for hopping ($E^{T}_{a,h}$ = 0.73 ± 0.04; see Table 1). For the estimation of the activation energy, we used an average temperature of our

https://doi.org/10.1021/jacs.1c09269
J. Am. Chem. Soc. 2021, 143, 18305−18316

Pt(111) experiments (500 K, which are most important to extraction of diffusion rates). This yielded an estimate of the hopping energy barrier: $E_{0,h}^{T}$ = 0.71 ± 0.04 eV, which also compares well with the DFT-derived hopping barrier obtained with the PBE functional and the estimated lower limit.

3.4. Comment about the 12% Rule for Diffusion Barriers. We notice that the Arrhenius expression-based prefactor derived for NH_3 hopping—$A_h^T = 10^{13.6\pm0.4}$ s^{-1}—is higher than values considered "common", i.e., $10^{<13}$ s^{-1}. However, this high value not only is in good agreement with DFT and cTST prediction of $10^{13.3}$ s^{-1} but also is physically reasonable. When a molecule is positioned at a weakly bound site, like the TS for hopping, its interaction with the surface is weakened, and thus the molecule is more likely to have an enhanced density of states and concomitant higher entropy. When the hopping barrier is very high, the TS is actually similar to a gas-phase molecule. Hence, the hopping prefactor will approach the prefactor for desorption, and the hopping of the molecule can be imagined to resemble transient or partial desorption, which is the case for NH_3 on Pt(111). Contrasting this to the case of a small hopping barrier, the adsorbates' density of states hardly changes at the hopping transition state compared to the molecule at its initial binding site. Therefore, the TST rate constant can be expressed using only the information about the molecule's hindered translational frequency, here, ∼120 cm^{-1}:

$$k(T) = \frac{k_B T}{h}\frac{1}{Q_x^{qHO}}\exp\left(-\frac{E_{hop,low}}{k_B T}\right) \xrightarrow{@500\ K} 10^{12.5} s^{-1}\exp\left(-\frac{E_{hop,low}}{k_B T}\right) \quad (3)$$

The associated prefactor will be in the range of 10^{12-13} s^{-1}, considered to be "typical". A similar conclusion was reached by Mavrikakis and co-workers[23,24] in developing the so-called 12% rule ($=E_{hop}/E_{bind}$) for diffusion barriers who argued that not only is the ratio of E_{hop} to E_{bind} likely to be about 0.12 but that the prefactors for hopping are commonly 10^{12-13} s^{-1}. Ammonia binding to and diffusion on Pt(111) is an illustrative example, emphasizing that one has to be cautious with drawing universal conclusions about scaling relations based on stable site binding energies alone, without considering the nuances of molecular structure. In Figure 4, we show for comparison the hopping rate constant with barrier estimated based on the 12% rule with the corresponding hopping prefactor from eq 3, where the failure of this estimate becomes evident.

It had been realized earlier that the choice of the adsorbate entropy[33,34,39,40] models and inclusion of anharmonic corrections[41] has a substantial impact on the prediction of thermodynamic state functions relevant for the description of reaction rates. However, coupling of different DOFs, which we clearly show to be important for NH_3 at Pt, is normally not considered. While these problems could, of course, be solved by demanding construction of a full dimensional potential energy surface, it is useful to develop a systematic hierarchy of correction schemes to provide an accurate description of thermal reaction rates using TST beyond the harmonic approximation. In that spirit, the application of the cTST model, incorporating the coupling of in-plane coordinates to different DOFs is a good step forward, especially as it requires little more input information from DFT than is already used for the less sophisticated approaches.

3.5. Implications for Modeling of the Ostwald Process. The ability of ammonia to find its way to steps is critical to it becoming chemically activated in the Ostwald process.[2,4,5,7] In principle, this may happen by either direct adsorption and desorption to and from steps or by adsorption at terraces followed by diffusion to steps in competition with desorption. The complexity of the adsorption/diffusion/desorption often goes unappreciated. In this section, we take up this matter.

3.5.1. Desorption Involving Multiple Active Sites. We have shown that NH_3 desorption from Pt(111) is primarily due to desorption from terraces, whereas the desorption rate from Pt(332) is strongly influenced by steps. In Figure 3a, we show the extracted first-order rate constants of NH_3 desorption from Pt(332) (black crosses) and compare them to the elementary rate constants for direct desorption from steps, k_d^S (orange dash-dotted line)—direct desorption from steps fails to explain experiment. This is easily understood as molecules bound at steps can readily hop first to a terrace site, where desorption is much faster. Simply put, hopping from steps to terraces with subsequent desorption from terraces involves two low barrier processes, whereas direct desorption from steps involves one high barrier process. By assuming a steady-state concentration of ammonia at terraces (conditions that are ensured for Pt(332) experiments; see section 3.5.2) and including competitive desorption from terraces and steps, we can derive the effective first-order desorption rate constant of NH_3 from a stepped surface (see section S8 of the SI for further details):

$$k_{eff}(T) = k_d^S + k_h^S(1-\mu)\times\frac{k_d^T}{k_h^T\mu + k_d^T} \quad (4)$$

where $k_{eff}(T)$ describes the "terrace-assisted" desorption of molecules (at low coverages) from surfaces with the step density, μ, which is defined as steps per unit cell length. The first term of eq 4 is the contribution of direct desorption from steps; the second term consists of a product between the hopping rate from steps to terraces, followed by the probability to desorb from terraces. For the derivation of this equation, we assumed that the total NH_3 population at Pt(332) is well described by the population at steps. This assumption is justified, as NH_3 has a high energy preference for steps, and entropic gain from binding at terraces is small due to a small number of terraces. See the SI section S8 for detailed derivation of this equation. The results of this "terrace-assisted" model are shown in Figure 3a as the green line, which agrees very well with the experimentally derived first-order desorption rate constants from Pt(332). In addition, the model reproduces the experimentally derived activation energy and prefactor for NH_3 desorption from Pt(332) quite well (see Figure 3d,e).

Figure 3a shows that desorption rates from an Ostwald catalyst with multiple active sites cannot be adequately described if exchange between steps and terraces is not explicitly considered. However, very often, kinetics modeling of the desorption process does not consider multiple binding sites even though they are present at the stepped model catalysts. Most commonly, single binding sites are assumed that have the characteristic energies and prefactors that are associated with the most stable binding site.[2,17,18] Clearly, this approach will underestimate the rate of actual desorption, where the adsorbate might exchange between binding sites and leave the surface through the less stable binding site. In fact, such

https://doi.org/10.1021/jacs.1c09269
J. Am. Chem. Soc. 2021, 143, 18305−18316

errors, even if the rate constants are modeled correctly, may lead to erroneous conclusions about the efficiency of a catalyst at the desired reaction conditions.

3.5.2. Limited Applicability of Mean-Field Approximation for NH_3 Chemistry at Pt. We have observed that the NH_3 desorption rate from Pt(111) with a step density of 0.4 ± 0.2% has a biexponential behavior, emerging from the competition between NH_3 desorption from terraces and its slow diffusion to steps. At Pt(332), we observe a single-exponential desorption rate, indicating that NH_3 equilibrates between steps and terraces, demonstrating that the competition between diffusion and desorption depends on the step density. Obviously, it will also depend on the temperature. Using the derived elementary process rate constants, we next investigate the competition between diffusion to steps and desorption from terraces as a function of the step density and temperature, including conditions relevant to Ostwald process.

For the purpose of demonstration, we determine NH_3's probability to reach a step after landing at the center of a terrace. To do so, we place a low initial concentration of NH_3 at the center of the terrace and solve the desorption−diffusion rate equations. We set $k_h^S = 0$, "freezing" the NH_3 molecule once it reaches a step. After all the NH_3 molecules have either desorbed from the terrace or diffused to the steps, we determine the fraction of molecules that remained at steps. The results of this analysis are shown in Figure 5.

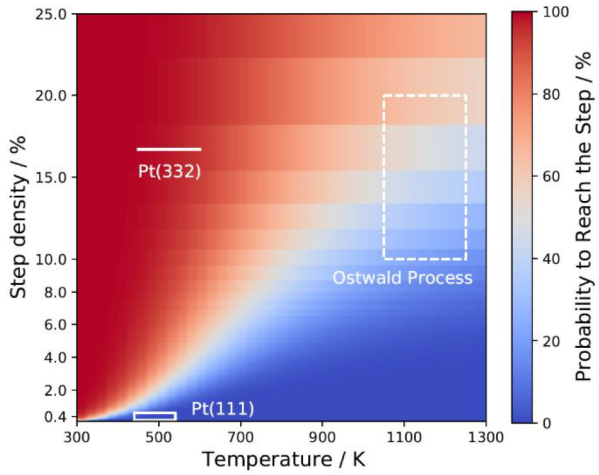

Figure 5. Probability of NH_3 molecules that landed in the center of the terrace to reach the steps before desorption as a function of step density and catalyst temperature. The temperature ranges (1050−1250 K) and associated step densities of our experimental (solid box) and Ostwald process (dashed box) conditions are indicated in the plot. The step densities for the Ostwald catalyst are not known, but we consider typical step/edge densities found on catalytic nanoparticles[42,43] as representative for real catalysts.

At low temperatures, diffusion to steps is fast compared to NH_3 desorption, and all molecules can reach the step. At high temperatures, NH_3 is less likely to reach the steps prior to desorption because the site-to-site hopping event approaches a time scale similar to that of the desorption event. Although the probability to reach the step increases with higher step densities, it can be clearly seen that at conditions typical for the Ostwald process not all molecules landing at majority terrace sites are able to reach the step prior to their desorption. It means that NH_3 must adsorb on or very close to a step site in order to react. Under typical Ostwald conditions, the reactants (NH_3* and O* at steps) are not able to encounter one another on a time scale faster than desorption, and as a consequence, the reactants cannot be assumed to be homogeneously mixed. This calls in question the basic assumption of the mean-field rate equations commonly used to model the Ostwald process.

The slow hopping rates and the previously observed preference for reaction at steps suggests that kinetics modeling of NH_3 chemistry at Pt needs to explicitly account for different active sites and accurately describe the exchange between them—factors that have not been considered in kinetics modeling of Ostwald process so far. Notice that under catalytically relevant conditions, other adsorbates like NO* and O* will be present at the catalyst and likely decrease NH_3's mobility even further. These results suggest that the key reaction in the Ostwald process may, in fact, be diffusion-limited, contradicting current models that assume fast diffusion.[2,4,5,18]

3.5.3. NH_3 Coverages at a Pt Catalyst under Ostwald Process Conditions. Current kinetics models for NH_3 oxidation at Pt lack transferability to reaction conditions different from those at which they were optimized. One possible reason for this is that the rate parameters employed do not describe elementary steps in the reaction. Using the experimentally derived desorption rates of this work, we can estimate the stationary NH_3 isosteres as a function of temperature and pressure at steps and terraces of a stepped Pt catalyst at conditions typical for the Ostwald process. We compare those with predictions of the KB[18] model that is frequently used for Ostwald process reactor simulations.[44−46]

This requires considering the coverage dependence of the ammonia desorption energy and prefactor. We use a coverage-dependent desorption barrier which we parametrize based on the experimentally derived NH_3 binding energy (in the zero-coverage limit) and the scaling of the binding energy with coverage derived from DFT calculations (see sections S5 and S9 of the SI). We have performed harmonic frequency and hopping barrier calculations with DFT at 0.06 and 0.25 ML NH_3 coverages, which allows us to estimate the coverage dependence of the prefactor. We assume that the logarithm of the prefactor—proportional to the entropy difference between the initial and transition state—scales linearly with coverage (see section S9 of the SI for further details). To test the constructed coverage-dependent desorption rate constant, we simulated TPD spectra from Pt(111) and compared them to results from previous works.[12] Earlier TPD studies[12] found broad NH_3 desorption peaks, indicating substantial adsorbate−adsorbate interactions, influencing the desorption rate. We find that our model predicts the right temperature ranges for the TPD spectra and accounts correctly for the coverage dependence, which is reflected by the shape of the TPD trace (see section S9 of the SI).

Next, we used the desorption−diffusion model to determine the steady-state NH_3 coverage at terraces and steps at surface temperatures and NH_3 partial pressures characteristic of the Ostwald process (see section S9 of the SI for details). We chose the highly stepped Pt(332) surface as a model catalyst for the Ostwald process. The results are shown in Figure 6 and compared to the KB model predictions.

We find that the steady-state coverage of NH_3 is strongly temperature- and pressure-dependent, whereas the KB model predicts saturated coverage under all conditions. Our model predicts rather low NH_3 coverages (blue color in Figure 6)

https://doi.org/10.1021/jacs.1c09269
J. Am. Chem. Soc. 2021, 143, 18305−18316

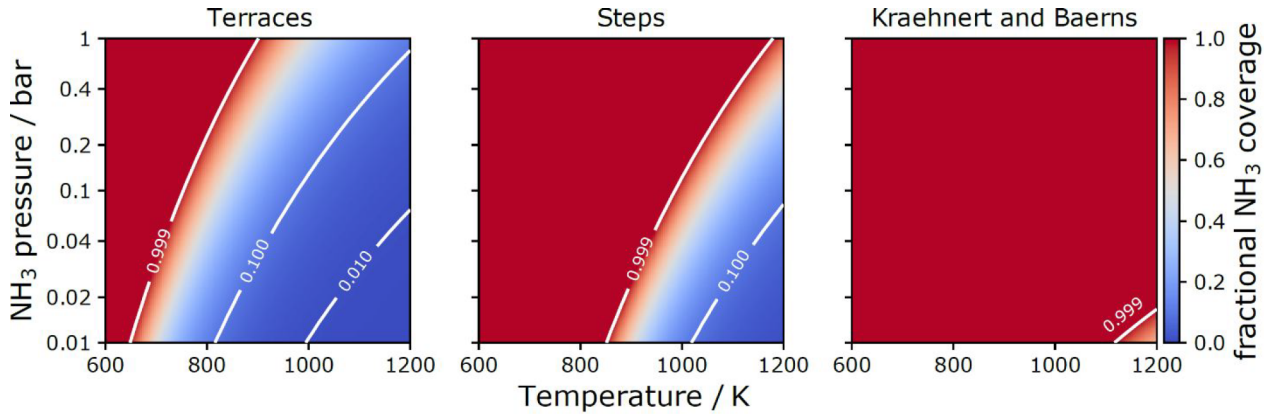

Figure 6. Fractional NH_3 coverages at terraces (left) and steps (middle) of a Pt(332) model catalyst at temperatures and NH_3 partial pressures typical for the Ostwald process. We compare our results (left and center panels) to the predictions of the KB model (right panel) which assumes one single active site for NH_3. Note that the Ostwald process is conducted at total pressures of ≥1 bar with NH_3 partial pressures of ∼10% of the total pressure.

over a broad range of Ostwald process conditions. We hasten to point out that NH_3 coverage will be strongly affected by coadsorbed O*, which can react to remove NH_3 but also may induce stronger ammonia binding to the surface. Still the comparisons shown in Figure 6 suggest that it is likely that the commonly applied kinetics model overpredicts the coverage of NH_3, which will lead to a higher degree of NH_3 slippage (where less nitrogen ends up as NO—the desired product of the Ostwald process). This is consistent with the fact that the KB model under-predicts the NO yield and tends to overestimate the N_2 yield at Ostwald process conditions.[18]

4. SUMMARY AND CONCLUSIONS

In this work, we have investigated the desorption kinetics of NH_3 from Pt(111) and Pt(332) between 430 and 620 K using velocity-resolved kinetics. Detailed analysis of NH_3 desorption kinetics using a diffusion−desorption kinetics model enabled us to extract rate constants for four elementary processes: direct desorption from terraces and from steps, site-to-site hopping at terraces, and hopping from steps to adjacent terrace sites. The measurement of a velocity-resolved kinetic trace provides simultaneously the speed distributions of desorbing molecules, from which we derive NH_3 thermal sticking coefficients to Pt using the principle of detailed balance.

The rate constants of the elementary processes of desorption and diffusion have been further analyzed using TST with DFT input parameters. The conventional TST models, which describe the partition function of the adsorbate with uncoupled DOFs, fail to reproduce the experimental results. A correction scheme to the partition function is implemented that allows NH_3 vibrational frequencies, associated with the molecule−surface interaction, to soften when displaced away from the most stable binding site. This approach faithfully reproduces the experimental kinetic data, and we derive accurate interaction energies for NH_3 at Pt surfaces, which we summarize in Table 3.

Our work provides compelling evidence that NH_3 diffusion on Pt(111) must pass over a large barrier, which is ∼65% of its binding energy. This is an exception to the so-called 12% rule. Instead of relying on such simple rules, our comparison with DFT calculations shows that the minimum energy path of diffusion appears to be highly accurate.

Table 3. Most Important Results for Ammonia Interactions at Pt Surfaces

NH_3/Pt interaction		recommended value
(111) desorption energy	$E^{T}_{0,d}$	1.13 ± 0.02 eV
(111) site-to-site hopping barrier	$E^{T}_{0,h}$	0.71 ± 0.04 eV
step preference over terrace	$\Delta E_{0,ST}$	0.23 ± 0.03 eV

Having a quantitatively accurate kinetics model for ammonia desorption and diffusion, we were able to critically evaluate the approximations commonly employed in kinetics modeling of the Ostwald process. It is known from previous work that NH_3 reacts efficiently with oxygen atoms at steps,[2,6,7] while reaction at terraces is less efficient. We show that at temperatures typical for the Ostwald process, the NH_3 hopping rate is close to its desorption rate, indicating that NH_3 landing at terrace sites is unlikely to reach the steps, where it may react prior to its desorption. This implies that mean-field kinetics models have limited applicability for prediction of NH_3 conversion rates and NO selectivity under Ostwald process conditions. Furthermore, by careful analysis of NH_3's desorption from Pt(332), we show that it is not possible to model the desorption rate from catalysts with multiple active sites by considering only the direct desorption from steps, an approach which is nevertheless persistently employed in kinetics modeling literature.[2,17]

With the help of DFT calculations, we extend the desorption rate constants beyond the zero-coverage limit of our experiment, which allows us to reproduce previously observed TPD spectra and to estimate NH_3 coverages at Ostwald process conditions. The comparison of our results with a kinetics model commonly used for reactor simulations provides a simple explanation why established models tend to overpredict the extent of NH_3 slip under Ostwald process conditions. We showed that this is a direct result of the model's prediction of high NH_3 coverages, which favor the formation of N_2 and N_2O and reduce the efficiency of NO formation.

In summary, the demonstrated approach exemplifies how the combination of high-quality kinetic data with TST analysis yields highly accurate elementary step rate constants, potentially capable of constructing mechanisms possessing high transferability without relying on empirical optimization within narrow range of experimental conditions.

https://doi.org/10.1021/jacs.1c09269
J. Am. Chem. Soc. 2021, 143, 18305−18316

5. METHODS

5.1. Experimental. The Pt surfaces (MaTeck GmbH) were prepared by sputtering with Ar^+ (3 keV) for 10 min and subsequent annealing at 1300 K for 20 min, and its cleanliness was verified with Auger electron spectroscopy. We employed two Pt(111) crystals with different step densities: the first had a step density quantified with atomic force microscopy of 0.4 ± 0.2% and the second a step density of 0.15 ± 0.05% estimated from the surface cut angle accuracy. We also used a Pt(332) crystal with a step density of 16.7%. Similar to previous work,[21,22,26] a 20−50 μs long pulsed molecular beam of NH_3 (0.5−2% NH_3 in He) passed from the source chamber through two differential pumping chambers before entering a surface-scattering chamber, with a base pressure of 2×10^{-10} mbar. The incidence kinetic energy of NH_3 in the beam was ∼0.25 eV. The NH_3 pulses (repetition rate 20−40 Hz) strike the Pt at an incidence angle of 30° from the surface normal. The dose provided by each NH_3 pulse was between 2×10^{-4} and 1×10^{-3} monolayer (ML).

Before investigating NH_3 desorption from Pt, we verified that NH_3 does not react under our conditions. We find no detectable H_2 or N_2 produced under our conditions. Isotopic exchange (e.g., NH_2D and HD, using NH_3 dosing of a D atom precovered Pt surfaces) was also absent. Furthermore, after dosing Pt(111) and Pt(332) surfaces with ∼2000 ML NH_3, no nitrogen signal could be detected in the Auger spectrum.

The desorbing and the directly scattered NH_3 were detected 2 cm from the surface using nonresonant multiphoton ionization (pulse duration 35 fs, average power 0.2 W, repetition rate 1 kHz). A pulsed homogeneous electric field, formed between two parallel flat meshes, projected the ions onto a time-gated MCP detector. The mass-to-charge ratio of the ions was selected with a time-gate on the microchannel plate (MCP), applied at a delay after pulsed extraction of the ions from the ionization region. The MCP amplified the ion signal, producing electrons that impinge upon a phosphor screen, emitting light recorded with a CCD camera. The pixel position provides information on the NH_3 velocity, which is used to convert NH_3 density to flux and to calculate the molecule's flight times to the surface and from surface to the ionizing laser spot. We integrated the flux images from 400 and 1200 m/s at angles close to the surface normal, which strongly suppresses the background from direct scattering, which peaks at an angle of ∼30° and a velocity of 1500 m/s. This integral was determined at many beam laser delays, which we correct to surface residence time, t_{res}, by subtracting the flight time, and we yield the kinetic trace $d[NH_3]/dt$ versus t_{res}. The translational energy distribution of the molecules could be obtained by summing ion images over all measured timings.

A fraction of the NH_3/Pt(332) data, from 453 to 553 K, was obtained in the 1 kHz detection setup and analyzed as has been described previously in detail.[25]

5.2. Computational. NH_3 binding energies, diffusion barriers, and frequencies at Pt(111) and Pt(332) have been obtained using the Vienna Ab-initio Simulation Package.[47−51] Periodic DFT calculations were performed at the level of generalized-gradient approximation using the PBE[30] exchange-correlation functional.

The core−electron interactions were described by the projector-augmented wave potentials,[52,53] with a cutoff energy of 400 eV for the plane-wave basis. The surfaces were modeled by a four-layer periodic slab, with each layer containing a 2 × 2 or a 4 × 4 supercell for Pt(111) and a 4 × 6 supercell for Pt(332). Two bottom layers were fixed during optimization. A 24 Å vacuum region was added to the slab to avoid interaction in the z-direction. The Brillouin zone was sampled with a 8 × 8 × 1 and a 5 × 5 × 1 with Γ-centered Monkhorst−Pack grids of special k-points for Pt(111) and Pt(332), respectively.

To predict adsorption energies, the two topmost surface layers and the NH_3 molecule were allowed to relax until forces were lower than 0.02 eV/Å. Accounting for the same amount of DOFs, the reaction paths and transition states for diffusion and desorption were located by the CI-NEB method.[31] The calculation was considered converged when forces were <0.05 eV/Å. The harmonic frequencies and normal modes were obtained solving the Hessian matrix for the DOFs of the NH_3 molecule, applying two central finite differences with displacements of 0.02 Å.

■ ASSOCIATED CONTENT

Supporting Information

The Supporting Information is available free of charge at https://pubs.acs.org/doi/10.1021/jacs.1c09269.

NH_3 speed distributions, analysis of sticking coefficients, comparison of desorption rates from Pt(111) with different step densities, equations for the diffusion−desorption kinetics model, coverage dependence of DFT-derived binding energies, construction of the partition functions for TST rate constant modeling, determination of first-order rate constants from experimental data, derivation of the terrace-assisted desorption model, construction of coverage-dependent desorption rate constants, and additional references (PDF)

■ AUTHOR INFORMATION

Corresponding Authors

Theofanis N. Kitsopoulos − *Institute for Physical Chemistry, Georg-August University of Goettingen, 37077 Goettingen, Germany; Department of Dynamics at Surfaces, Max Planck Institute for Biophysical Chemistry, 37077 Goettingen, Germany; Department of Chemistry, University of Crete, 71003 Heraklion, Greece; Institute of Electronic Structure and Laser − FORTH, 71110 Heraklion, Greece;* orcid.org/0000-0001-6228-1002; Email: theo.kitsopoulos@mpibpc.mpg.de

Alec M. Wodtke − *Institute for Physical Chemistry, Georg-August University of Goettingen, 37077 Goettingen, Germany; Department of Dynamics at Surfaces, Max Planck Institute for Biophysical Chemistry, 37077 Goettingen, Germany; International Center for Advanced Studies of Energy Conversion, Georg-August University of Goettingen, 37077 Goettingen, Germany;* orcid.org/0000-0002-6509-2183; Email: alec.wodtke@mpibpc.mpg.de

Authors

Dmitriy Borodin − *Institute for Physical Chemistry, Georg-August University of Goettingen, 37077 Goettingen, Germany; Department of Dynamics at Surfaces, Max Planck Institute for Biophysical Chemistry, 37077 Goettingen, Germany*

Igor Rahinov − *Department of Natural Sciences, The Open University of Israel, 4353701 Raanana, Israel*

Oihana Galparsoro − *Donostia International Physics Center (DIPC), 20018 Donostia-San Sebastián, Spain; Kimika Fakultatea, Euskal Herriko Unibertsitatea UPV/EHU, P.K. 1072 Donostia-San Sebastián, Spain*

Jan Fingerhut − *Institute for Physical Chemistry, Georg-August University of Goettingen, 37077 Goettingen, Germany*

Michael Schwarzer − *Institute for Physical Chemistry, Georg-August University of Goettingen, 37077 Goettingen, Germany*

Kai Golibrzuch − *Department of Dynamics at Surfaces, Max Planck Institute for Biophysical Chemistry, 37077 Goettingen, Germany*

Georgios Skoulatakis − *Department of Dynamics at Surfaces, Max Planck Institute for Biophysical Chemistry, 37077 Goettingen, Germany*

Daniel J. Auerbach − *Department of Dynamics at Surfaces, Max Planck Institute for Biophysical Chemistry, 37077 Goettingen, Germany*

Alexander Kandratsenka − *Department of Dynamics at Surfaces, Max Planck Institute for Biophysical Chemistry, 37077 Goettingen, Germany;* orcid.org/0000-0003-2132-1957

Dirk Schwarzer − *Department of Dynamics at Surfaces, Max Planck Institute for Biophysical Chemistry, 37077 Goettingen, Germany;* orcid.org/0000-0003-3838-2211

Complete contact information is available at: https://pubs.acs.org/10.1021/jacs.1c09269

Funding

Open access funded by Max Planck Society.

Notes

The authors declare no competing financial interest.

■ ACKNOWLEDGMENTS

D.B. and M.S. thank the BENCh graduate school, funded by the DFG (389479699/GRK2455). I.R. gratefully acknowledges the support by Israel Science Foundation, ISF (Grant No. 2187/19), and by the Open University of Israel Research Authority (Grant No. 31044). O.G. acknowledges financial support by the Spanish Ministerio de Ciencia e Innovación (Grant No. PID2019-107396GB-I00/AEI/10.13039/501100011033). T.N.K., G.S., M.S., and J.F. acknowledge support from the European Research Council (ERC) under the European Union's Horizon 2020 research and innovation program (Grant Agreement No. 833404).

■ REFERENCES

(1) Bartholomew, C. H.; Farrauto, R. J. *Fundamentals of Industrial Catalytic Processes*; Wiley, 2005; Vol. 2, pp 570−575.

(2) Ma, H. Y.; Schneider, W. F. Structure- and Temperature-Dependence of Pt-Catalyzed Ammonia Oxidation Rates and Selectivities. *ACS Catal.* **2019**, *9* (3), 2407−2414.

(3) Rafti, M.; Vicente, J. L.; Albesa, A.; Scheibe, A.; Imbihl, R. Modeling ammonia oxidation over a Pt (533) surface. *Surf. Sci.* **2012**, *606* (1−2), 12−20.

(4) Imbihl, R.; Scheibe, A.; Zeng, Y. F.; Gunther, S.; Kraehnert, R.; Kondratenko, V. A.; Baerns, M.; Offermans, W. K.; Jansen, A. P. J.; van Santen, R. A. Catalytic ammonia oxidation on platinum: mechanism and catalyst restructuring at high and low pressure. *Phys. Chem. Chem. Phys.* **2007**, *9* (27), 3522−3540.

(5) Weststrate, C. J.; Bakker, J. W.; Rienks, E. D. L.; Vinod, C. P.; Matveev, A. V.; Gorodetskii, V. V.; Nieuwenhuys, B. E. Ammonia oxidation on Pt(410). *J. Catal.* **2006**, *242* (1), 184−194.

(6) Gland, J. L.; Woodard, G. C.; Korchak, V. N. Ammonia Oxidation on the Pt(111) and Pt(S)-12(111) x (111) Surfaces. *J. Catal.* **1980**, *61* (2), 543−546.

(7) Gland, J. L.; Korchak, V. N. Ammonia Oxidation on a Stepped Platinum Single-Crystal Surface. *J. Catal.* **1978**, *53* (1), 9−23.

(8) Gland, J. L. Adsorption and Decomposition of Nitric-Oxide and Ammonia on a Stepped Platinum Single-Crystal Surface. *Surf. Sci.* **1978**, *71* (2), 327−350.

(9) Guthrie, W. L.; Sokol, J. D.; Somorjai, G. A. The Decomposition of Ammonia on the Flat (111) and Stepped (557) Platinum Crystal-Surfaces. *Surf. Sci.* **1981**, *109* (2), 390−418.

(10) Szulczewski, G.; Levis, R. J. Collision-Induced Desorption of Ammonia Chemisorbed on Pt(111) - from Direct Measurement of the Threshold Energy to Determination of the Surface-Adsorbate Bond Strength. *J. Chem. Phys.* **1995**, *103* (23), 10238−10251.

(11) Cai, L.; Xiao, X. D.; Loy, M. M. T. Desorption of polyatomic molecules from the Pt(111) surface by femtosecond laser radiation. *J. Chem. Phys.* **2001**, *115* (20), 9490−9495.

(12) Mieher, W. D.; Ho, W. Thermally Activated Oxidation of NH3 on Pt(111) - Intermediate Species and Reaction-Mechanisms. *Surf. Sci.* **1995**, *322* (1−3), 151−167.

(13) Sexton, B. A.; Mitchell, G. E. Vibrational-Spectra of Ammonia Chemisorbed on Platinum (111) 0.1. Identification of Chemisorbed States. *Surf. Sci.* **1980**, *99* (3), 523−538.

(14) Wellendorff, J.; Silbaugh, T. L.; Garcia-Pintos, D.; Norskov, J. K.; Bligaard, T.; Studt, F.; Campbell, C. T. A benchmark database for adsorption bond energies to transition metal surfaces and comparison to selected DFT functionals. *Surf. Sci.* **2015**, *640*, 36−44.

(15) Offermans, W. K.; Jansen, A. P. J.; van Santen, R. A. Ammonia activation on platinum {111}: A density functional theory study. *Surf. Sci.* **2006**, *600* (9), 1714−1734.

(16) Novell-Leruth, G.; Ricart, J. M.; Perez-Ramirez, J. Pt(100)-catalyzed ammonia oxidation studied by DFT: Mechanism and microkinetics. *J. Phys. Chem. C* **2008**, *112* (35), 13554−13562.

(17) Ma, H. Y.; Schneider, W. F. DFT and microkinetic comparison of Pt, Pd and Rh-catalyzed ammonia oxidation. *J. Catal.* **2020**, *383*, 322−330.

(18) Kraehnert, R.; Baerns, M. Kinetics of ammonia oxidation over Pt foil studied in a micro-structured quartz-reactor. *Chem. Eng. J.* **2008**, *137* (2), 361−375.

(19) Scheuer, A.; Votsmeier, M.; Schuler, A.; Gieshoff, J.; Drochner, A.; Vogel, H. NH3-Slip Catalysts: Experiments Versus Mechanistic Modelling. *Top. Catal.* **2009**, *52* (13−20), 1847−1851.

(20) Serri, J. A.; Tully, J. C.; Cardillo, M. J. The influence of steps on the desorption kinetics of NO from Pt(111). *J. Chem. Phys.* **1983**, *79* (3), 1530−1540.

(21) Borodin, D.; Rahinov, I.; Fingerhut, J.; Schwarzer, M.; Hörandl, S.; Skoulatakis, G.; Schwarzer, D.; Kitsopoulos, T. N.; Wodtke, A. M. NO Binding Energies to and Diffusion Barrier on Pd Obtained with Velocity-Resolved Kinetics. *J. Phys. Chem. C* **2021**, *125* (21), 11773−11781.

(22) Neugebohren, J.; Borodin, D.; Hahn, H. W.; Altschaffel, J.; Kandratsenka, A.; Auerbach, D. J.; Campbell, C. T.; Schwarzer, D.; Harding, D. J.; Wodtke, A. M.; Kitsopoulos, T. N. Velocity-resolved kinetics of site-specific carbon monoxide oxidation on platinum surfaces. *Nature* **2018**, *558* (7709), 280−283.

(23) Peng, G. W.; Mavrikakis, M. Adsorbate Diffusion on Transition Metal Nanoparticles. *Nano Lett.* **2015**, *15* (1), 629−634.

(24) Nilekar, A. U.; Greeley, J.; Mavrikakis, M. A simple rule of thumb for diffusion on transition-metal surfaces. *Angew. Chem., Int. Ed.* **2006**, *45* (42), 7046−7049.

(25) Borodin, D.; Golibrzuch, K.; Schwarzer, M.; Fingerhut, J.; Skoulatakis, G.; Schwarzer, D.; Seelemann, T.; Kitsopoulos, T.; Wodtke, A. M. Measuring Transient Reaction Rates from Nonstationary Catalysts. *ACS Catal.* **2020**, *10* (23), 14056−14066.

(26) Harding, D. J.; Neugebohren, J.; Hahn, H.; Auerbach, D. J.; Kitsopoulos, T. N.; Wodtke, A. M. Ion and velocity map imaging for surface dynamics and kinetics. *J. Chem. Phys.* **2017**, *147* (1), 013939.

(27) Rettner, C. T.; Schweizer, E. K.; Mullins, C. B. Desorption and Trapping of Argon at a 2H-W(100) Surface and a Test of the Applicability of Detailed Balance to a Nonequilibrium System. *J. Chem. Phys.* **1989**, *90* (7), 3800−3813.

(28) Borodin, D.; Rahinov, I.; Shirhatti, P. R.; Huang, M.; Kandratsenka, A.; Auerbach, D. J.; Zhong, T.; Guo, H.; Schwarzer, D.; Kitsopoulos, T. N.; Wodtke, A. M. Following the microscopic pathway to adsorption through chemisorption and physisorption wells. *Science* **2020**, *369* (6510), 1461−1465.

(29) King, D. A. Surface-Diffusion of Adsorbed Species - a Review. *J. Vac. Sci. Technol.* **1980**, *17* (1), 241−247.

(30) Perdew, J. P.; Burke, K.; Ernzerhof, M. Generalized gradient approximation made simple. *Phys. Rev. Lett.* **1996**, *77* (18), 3865−3868.

(31) Henkelman, G.; Uberuaga, B. P.; Jonsson, H. A climbing image nudged elastic band method for finding saddle points and minimum energy paths. *J. Chem. Phys.* **2000**, *113* (22), 9901−9904.
(32) Engelhart, D. P.; Wagner, R. J. V.; Meling, A.; Wodtke, A. M.; Schafer, T. Temperature programmed desorption of weakly bound adsorbates on Au(111). *Surf. Sci.* **2016**, *650*, 11−16.
(33) Sprowl, L. H.; Campbell, C. T.; Arnadottir, L. Hindered Translator and Hindered Rotor Models for Adsorbates: Partition Functions and Entropies. *J. Phys. Chem. C* **2016**, *120* (18), 9719−9731.
(34) Jørgensen, M.; Grönbeck, H. Adsorbate Entropies with Complete Potential Energy Sampling in Microkinetic Modeling. *J. Phys. Chem. C* **2017**, *121* (13), 7199−7207.
(35) McClurg, R. B.; Flagan, R. C.; Goddard, W. A. The hindered rotor density-of-states interpolation function. *J. Chem. Phys.* **1997**, *106* (16), 6675−6680.
(36) Garcia-Hernandez, M.; Lopez, N.; Moreira, I. D.; Paniagua, J. C.; Illas, F. Ab initio cluster model approach to the chemisorption of NH3 on Pt(111). *Surf. Sci.* **1999**, *430* (1−3), 18−28.
(37) Tully, J. C. The Dynamics of Adsorption and Desorption. *Surf. Sci.* **1994**, *299* (1−3), 667−677.
(38) Novell-Leruth, G.; Valcarcel, A.; Clotet, A.; Ricart, J. M.; Perez-Ramirez, J. DFT characterization of adsorbed NHx species on Pt(100) and Pt(111) surfaces. *J. Phys. Chem. B* **2005**, *109* (38), 18061−18069.
(39) Bajpai, A.; Mehta, P.; Frey, K.; Lehmer, A. M.; Schneider, W. F. Benchmark First-Principles Calculations of Adsorbate Free Energies. *ACS Catal.* **2018**, *8* (3), 1945−1954.
(40) Campbell, C. T.; Sprowl, L. H.; Árnadóttir, L. Equilibrium Constants and Rate Constants for Adsorbates: Two-Dimensional (2D) Ideal Gas, 2D Ideal Lattice Gas, and Ideal Hindered Translator Models. *J. Phys. Chem. C* **2016**, *120* (19), 10283−10297.
(41) Amsler, J.; Plessow, P. N.; Studt, F.; Bucko, T. Anharmonic Correction to Adsorption Free Energy from DFT-Based MD Using Thermodynamic Integration. *J. Chem. Theory Comput.* **2021**, *17* (2), 1155−1169.
(42) Groot, I. M. N.; Kleyn, A. W.; Juurlink, L. B. F. Separating Catalytic Activity at Edges and Terraces on Platinum: Hydrogen Dissociation. *J. Phys. Chem. C* **2013**, *117* (18), 9266−9274.
(43) García-Diéguez, M.; Hibbitts, D. D.; Iglesia, E. Hydrogen Chemisorption Isotherms on Platinum Particles at Catalytic Temperatures: Langmuir and Two-Dimensional Gas Models Revisited. *J. Phys. Chem. C* **2019**, *123* (13), 8447−8462.
(44) Shrestha, S.; Harold, M. P.; Kamasamudram, K. Experimental and modeling study of selective ammonia oxidation on multifunctional washcoated monolith catalysts. *Chem. Eng. J.* **2015**, *278*, 24−35.
(45) Scheuer, A.; Hirsch, O.; Hayes, R.; Vogel, H.; Votsmeier, M. Efficient simulation of an ammonia oxidation reactor using a solution mapping approach. *Catal. Today* **2011**, *175* (1), 141−146.
(46) Wiser, A. Investigation of the industrial NH3 oxidation by CFD simulations including detailed surface kinetics. Ph.D. Thesis, TU Darmstadt, 2020.
(47) Kresse, G.; Hafner, J. Abinitio Molecular-Dynamics for Liquid-Metals. *Phys. Rev. B: Condens. Matter Mater. Phys.* **1993**, *47* (1), 558−561.
(48) Kresse, G.; Hafner, J. Ab-Initio Molecular-Dynamics Simulation of the Liquid-Metal Amorphous-Semiconductor Transition in Germanium. *Phys. Rev. B: Condens. Matter Mater. Phys.* **1994**, *49* (20), 14251−14269.
(49) Kresse, G.; Hafner, J. Norm-Conserving and Ultrasoft Pseudopotentials for First-Row and Transition-Elements. *J. Phys.: Condens. Matter* **1994**, *6* (40), 8245−8257.
(50) Kresse, G.; Furthmuller, J. Efficient iterative schemes for ab initio total-energy calculations using a plane-wave basis set. *Phys. Rev. B: Condens. Matter Mater. Phys.* **1996**, *54* (16), 11169−11186.
(51) Kresse, G.; Furthmuller, J. Efficiency of ab-initio total energy calculations for metals and semiconductors using a plane-wave basis set. *Comput. Mater. Sci.* **1996**, *6* (1), 15−50.
(52) Blöchl, P. E. Projector Augmented-Wave Method. *Phys. Rev. B: Condens. Matter Mater. Phys.* **1994**, *50* (24), 17953−17979.
(53) Kresse, G.; Joubert, D. From ultrasoft pseudopotentials to the projector augmented-wave method. *Phys. Rev. B: Condens. Matter Mater. Phys.* **1999**, *59* (3), 1758−1775.

https://doi.org/10.1021/jacs.1c09269
J. Am. Chem. Soc. 2021, 143, 18305−18316